System development for improvement of quality inspection and control in the food industry

Rodrigo Alves Lopes

rodrigo.alves.lopes@tecnico.ulisboa.pt

Instituto Superior Técnico, Universidade de Lisboa, Lisboa, Portugal

June 2019

ABSTRACT

The objective of this thesis is to identify a system capable of in-line inspection of BOPP film sealing quality in straw packaging, leading to the detection and containment of defective products. In this work, the sealing process principle and the parameters that govern the process are studied. Sealed film samples, collected with different process parameters in an industrial environment, are initially classified according to their seal strength with an off-line peel test. For in-line inspection, two distinct solutions are proposed. A system for the measurement of film temperature after sealing using infrared pyrometers is studied and its correlation with seal strength variation is analyzed. A system based on machine vision is also studied, where sample images are acquired with an infrared lighting system and a polarized filtering system. For image features extraction, two textural descriptors are proposed based on the local binary pattern and the gray level co-occurrence matrix and for classification, a multi-layer perceptron neural network is used. The capabilities of both systems in accurately identifying film sealing defects are analyzed.

Keywords: *Sealing, BOPP film, In-line inspection, Pyrometer, Infrared lighting, Polarized filter, Texture.*

1. Introduction

1.1 Overview

The primary function of a package is to protect the product, through transportation, until its use. To better achieve this, packaging materials and processes have evolved through the years, to meet the changing needs of the industries and the consumers.

it wasn't until the 20th century that plastic subtracts appeared as a solution, with the introduction of cellophane marking the beginning of the modern era of flexible packaging. Biaxially Oriented Polypropylene, known as BOPP, was first developed in 1961. Polypropylene is a thermoplastic characterized by low density and good resistance to chemicals and to mechanical fatigue, being also an excellent moisture barrier. This material is commonly oriented to improve optical, mechanical, and barrier properties, becoming transparent, which makes it very useful for packaging.

For the food industry, which englobes not only food products, but products that come into contact with them, packaging gains big importance, being responsible for blocking any type of product contamination and avoiding harmful microbe growth, preventing spoilage and extending the shelf life. In order to prevent the product from being contaminated, a good package seal is required, to be able to withstand the extreme environments it may be subjected to during shipping and handling. High altitudes may put pressure on the seal as the package expands due to the thinning of the air surrounding it, while extreme temperature variations may affect seal durability.

Over the years, the consumer importance given to the product quality has been increasing. This, together with the more restrict quality norms and regulations imposed to the industries, has seen companies investing in product quality assurance. This trend also applies to packaging, specially sealing quality. Companies have been motivated to look for and developed new and improved systems for sealing quality inspection. From the companies' point of view, sample testing is not enough anymore, and 100% quality inspection needs to be guaranteed. This is the base motivation for this thesis, which tries to propose different methods for in-line inspection of the film seal quality of straws packaging [1]–[3].

1.2 Sealing quality inspection methods

Over the years several approaches for film sealing quality inspection have been developed. The most common forms of seal inspection still focus on destructive test methods applied to package samples, such as burst testing or tensile testing. These methods, however, can only be applied to a small number of samples, making the detection of sporadic defects difficult. Because of this, companies have looked over the years for the search and development of in-line seal inspection systems, which should be non-destructive, fast and contactless.

Multiple methods of sealing inspection, based on different quality requisites, have been proposed throughout the years. Pascall et al.(2002) presented a study where the effectiveness of ultrasonic imaging for non-destructive assessment of seal strength in polymeric trays was investigated [4]. Ostyn et al. (2007) were able to detect wrinkles and solid contaminants in seals based on the analysis of the vibration pattern of sealing bars applied to statistical process control [5]. Morita et al. (2007) explored the potential of terahertz radiation in seal inspection while Song et al. (2014) evaluated the capabilities of high voltage in leak detection of flexible pouches [6].

From all the methods proposed, machine vision has been one of the most analyzed solutions. These systems have evolved significantly with the technology advances to tackle the challenges from modern

manufacturing industry. Shuangyang (2010) studied the inspection of seal quality using machine vision [7]. Examples of acceptable and non-acceptable food packing seals images were analyzed, their uniformity was examined and associated with numerical quality measures and template matching was used for classification. Barnes et al. (2012) presented two imaging systems for detecting faults in heat seals of polymer trays, one using polarized light stress analysis and the other based on laser scatter imaging [8]. From the images obtained, the seal area was segmented and a very large set of candidate features, based on statistical information related to color and texture, was extracted. An adaptive boosting algorithm was then used to automatically select the best features and a classifier was trained to detected faults in different regions of the seal.

Thermal imaging is also a method that appeared as an application in sealing inspection when smaller systems started to become available, enabling the use of infrared imaging for commercial and industrial applications. D'huys et al. (2016) studied the use of an active thermography method for seal contamination detection, where six different thermal image processing methods were compared [9].

2. Sealing process

The sealing process were plastic straws are wrapped in BOPP film will be the focus of this work.

2.1 Packaging film

The film used is made of coextruded bi-oriented polypropylene (BOPP), a thermoplastic characterized by low density and good resistance to chemicals and to mechanical fatigue, including environmental stress cracking.

The most important film characteristic relevant to this work is its thickness. The film's sealing initiation temperature is 105ºC, at which the heat sealable layer starts to melt, which means that it is required for the film to reach at least this temperature for sealing to occur. In this thesis two different combinations of film will be analyzed.

Clear film will be the term used in reference to the use of two layers of BOPP film sealed together. These have a thickness of 18 µm and present a clear pattern throughout. When the term rugged film is used in this work, it is in reference to the use of two layers of BOPP film sealed together, each with a thickness of 16 µm. The term rugged is chosen due to the film presenting, after sealing, a striped pattern.

Figure 1- On the left: sample of clear film; on the right: sample of rugged film.

2.2 Heat sealing process

In this process, the straws are placed between two layers of film, which are sealed together between two cylinders under pressure, where the sealing cylinder is heated at enough temperature to trigger the sealing process. Given enough time and pressure, molecular segments diffuse across the interface and reorganize, forming entanglements within the polymer chains, destroying the interface and producing a homogenous layer that remains homogeneous after cooling, resulting in a chemical bond.

Sealing quality problems are a consequence of an error in the three main defining parameters: temperature, dwell time and pressure.

The temperature parameter corresponds to the temperature of the sealing roll surface when it comes in contact with the film. Dwell time refers to the period of time where the sealing roll is in contact with the film. Both of these parameters are directly related to the amount of heat that is transferred to the sealing interface. If either are not high enough, the sealing layer might not achieve the sealing initiation temperature required for sealing to start.

The third parameter is the pressure at which the equipment brings together and holds the two films to form the seal. If not enough pressure is applied, the real contact area decreases significantly, decreasing the thermal contact conductance coefficient, which has a negative impact in the heat transferred to the film.

Changes in these parameters can produce significant variability in seal strength.

2.3 Sealing defects

Sealing defects occur when the sealing strength is lower than the tolerance defined. This corresponds to the force necessary to separate both films after sealing. When this strength is low, we have what we call weak sealing, where it is easier to open the straw pouch. Any small force, either from product transportation or application in the package, can make the straw pocket open, leaving the straw vulnerable to contamination, creating a health hazard for the consumer.

2.4 Sealing strength analysis

In order to characterize the sealing defects, differentiating good from weak sealing, it is required to analyze the film sealing strength. Due to the high norms and restrictions that industries are subject to, standards for seal strength analysis are set in place worldwide.

For this analysis, it will be taken into account the ISO 11607-1:2019 norm, which includes the ASTM F88 procedure that describes the use of a peel test, where small rectangular shaped samples of the sealed film should be collected and each film slowly striped apart from each other, collecting data related to the maximum force required for the film's separation.

2.4.1 Critical area identification

From the results obtained for samples at different zones of the film, it was possible to conclude that the critical area is present at the film edges, next to the straw corrugation. This is a consequence of the uneven heating distribution at the sealing cylinder surface. This critical area will be the focus for the next chapters.

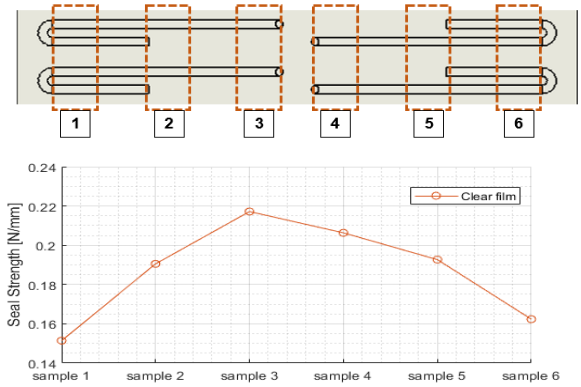

Figure 2- Critical area identified with the lowest seal strength.

2.4.1 Sealing parameters variation results

Having identified the critical area, samples were obtained from varying the sealing parameters.

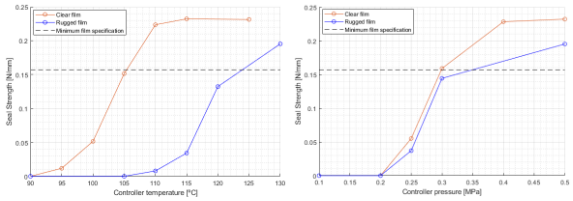

Figure 3- Evolution of seal strength for both types of films with temperature variation on the left, and pressure variation on the right.

From figure 3 it is possible to conclude that good sealing is only considered for temperature and pressure conditions where the seal strength reaches a plateau value. This is the value considered by the factory as standard. Any deviation from it, even if still close to the film's minimum specifications, should not be approved and should be identified as not valid.

3. Film Temperature Analysis

The sealing process is responsible for transmitting energy to the BOPP films being sealed together. All the parameters responsible for a good sealing process have an influence on the amount of heat that is transferred to the films, as described in equation 1.

$$\frac{\Delta Q}{\Delta t} = \frac{T_{sr} - T_b}{\frac{1}{h_{c1}.A} + \frac{\Delta x}{k.A} + \frac{1}{h_{c2}.A} + \frac{\Delta x}{k.A}} \qquad \text{Eq. 1}$$

The total heat transferred can also be directly related to the temperature that the film reaches at the end of the sealing process. This condition allows us to relate the quality of the seal with the final temperature of the film after sealing. This hypothesis will be the base of the work described in this chapter. In order to inspect the product sealing quality by measuring the film temperature at the end of the process, a system with an infrared pyrometer will be analyzed.

3.1 Radiation pyrometry

Radiation pyrometry is a powerful method of temperature measurement based on a simple principle: every body at a temperature superior to the absolute zero (> 0 K) emits electromagnetic radiation [10]. Analyzing the radiation emitted allows the estimation of the body surface temperature.

This is where pyrometry methods bring a huge advantage in comparison to more conventional ones, since they do not need mechanical contact with the inspected component and provide an almost instant measure of the temperature value.

3.2 Pyrometers

A pyrometer is a device that can measure the temperature of a small surface area. It is constituted by an optical system, which picks up the thermal radiation emitted from a circular surface area and focuses it on a detector. The temperature value measured results in an average of the area inspected [11].

For an application on thin BOPP film, due to some of the film inherit properties, in order to achieve a valid measurement, several conditions must be met.

Film emissivity is a parameter that needs to be precisely defined for accurate measurements. A simple way to estimate this parameter is based on Kirchhoff's law. Emissivity depends on the values of reflectivity and transmissivity.

When it comes to plastics, a good approximation for reflectivity is 0.04, independent of wavelength and material thickness.

The transmissivity value is dependent not only on the wavelength of radiation, but also on the type of material and object thickness. It is most effective to design an installation which results in using the highest emissivity value possible. When it comes to thin-film plastics, they tend to be transparent at many wavelengths, which relates to high transmissivity values. This allows radiation from objects behind the film to pass through and influence the measured intensity. To contradict this situation, the wavelength measured by the device should be carefully selected, to assure that the transmissivity value is as low as possible.

The study relating the wavelength of radiation with the transmissivity of the polypropylene has been developed in controlled conditions, concluding that the transmissivity reaches values close to zero only for a wavelength of 3.43 μm. Due to the importance of this parameter, special pyrometers have been developed by companies focused in this technology, that are specially designed for the temperature measurement of thin polypropylene film and only measure in this specific wavelength.

Assuming the transmissivity value as zero in this wavelength, we can estimate the emissivity value as 0.96.

3.3 Pyrometer in sealing inspection

In spite of only being able to obtain the temperature value of what is basically a single surface point in time, this does not invalidate their use in film sealing inspection. As previously mentioned, it is not necessary to obtain the entire surface temperature distribution to reach a conclusion regarding quality of seal, since due to the heating distribution in the sealing process, sealing defects always appear first in the critical area. As such, it can be assumed that inspecting the temperature in this area is enough to evaluate the sealing quality.

Since a pyrometer is capable of measuring the temperature in a certain spot in a specific period of time, as the continuous of film and straws produced pass through the pyrometer inspection field of view, it is possible to obtain the temperature values of the critical area over time and relate it to sealing quality.

To test this assumption, a pyrometer Optris® CTP3 was used. This sensor was specially developed for precise temperature measurements of thin plastic films, detecting radiation only in the 3.43 μm wavelength. Due to its optical parameters, it should be placed at 30 mm or less from the film, in a direction normal to the film surface, since this direction corresponds to its highest emissivity point.

3.4 Pyrometer model

In order to predict how the pyrometer will behave in measuring the film surface temperature after sealing, during normal production, its model and temperature response were studied.

A pyrometer, just like most temperature sensors, can be estimated as a first-order system, in whose input-output equation is a first order differential equation.

$$G(s) = \frac{1}{Ts+1} \qquad \text{Eq. 2}$$

To define the system model, time constant *T* must be estimated. This will be done in two different ways, a theoretical way where the constant used is the one present in the pyrometer datasheet, and an experimental way where the time constant is estimated.

3.4.1 Theoretical model

In the sensor datasheet, the settling time equals 100 ms, corresponding to a constant time of 25 ms. From this it is possible to obtain the model in equation 2.

$$G_{tc}(s) = \frac{1}{25s+1} \qquad \text{Eq. 3}$$

3.4.2 Experimental model

In order to estimate the sensor response time, an experiment was conducted where a sample of film with straws was placed in a hoven and heated at 68ºC for 15 minutes, giving it enough time to reach this temperature uniformly. The sensor is placed normal to the film surface and covered by an object at room temperature. After the temperature of the film is stable, the hoven door is opened, and the object blocking the sensor is removed. The sensor is subjected to a temperature variation between room temperature and film temperature and its response over time is saved for processing. From the results, the model shown in equation 4 was obtained.

$$G_{ec}(s) = \frac{1}{22.94s+1} \qquad \text{Eq. 4}$$

3.5 Pyrometer theoretical response

Having calculated the pyrometer model, it is possible to estimate its response during straw production.

3.5.1 Production model

To measure the film surface temperature, the pyrometer is fixed normal to the film surface. The sensor, however, doesn't measure only a single spot but a small area. The temperature value measured results in an average of the area inspected.

With the sensor fixed, as the film passes through, the area measured includes sealed film and non-sealed film (pouch area). As such, the temperature values obtained will not be constant, but oscillate between a low and a high temperature value. When estimating the temperature variation, it is assumed that each area, sealed and non-sealed, presents a uniform temperature throughout.

As the film passes through the pyrometer measurement area, part of this area belongs to sealed film, while the other belongs to non-sealed film. The ratio between these parts can be estimated based on the circular segment area mathematical formula, described in equation 5 and represented in figure 4.

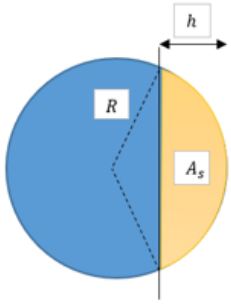

Figure 4- Circular segment representation.

$$A_s = R^2 \cos^{-1}\left(\frac{R-h}{R}\right) - (R-h)\sqrt{2Rh-h^2} \qquad \text{Eq. 5}$$

Knowing the circular segment area, we can relate it with the total measurement area to obtain the ratio between temperatures over time.

$$r(t) = \frac{A_s(t)}{A_p} \qquad \text{Eq. 6}$$

3.5.2 Pyrometer response

Having estimated the pyrometer model and knowing the theoretical surface temperature variation of the film, it is possible to analyze the model dynamic response for this input.

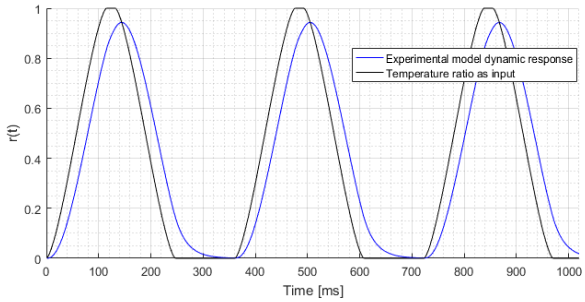

Figure 5- Simulation of the pyrometer model time response

It is possible to see that the system model cannot keep up with the surface temperature variation. Due to the production high velocity and the small distance between straws, the pyrometer is not exposed enough time to the sealed film between straws to reach the sealing maximum temperature. A constant error of 5.68% is always present.

4. Film Sealing Imaging

Another solution for sealing quality inspection involves using machine vision.

In this chapter, two different systems for sealed film image collecting will be presented together with two different image descriptor methods based on texture analysis.

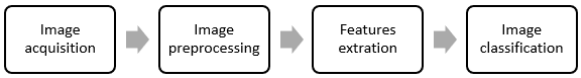

Figure 6- Imaging processing steps.

4.1 Image acquisition

In this work, two different types of image acquisition setups will be tested, with tools designed to possibly collect the film characteristics necessary for its right classification.

4.1.1 Infrared imaging system

One of the most used types of lighting revolves around infrared radiation, which is generally invisible to the human eye. It can be used in innumerous machine vision applications where the specific properties of this lighting bring major advantages, such as transmitting through certain materials and neutralizing contrast differences. In this system, infrared backlight was used, together with a collimated filter and two cameras, in parallel, to inspect both straws side by side. These are CMOS area scan monochromatic cameras which have a capability of 38.8 fps, enough to keep up with the production line.

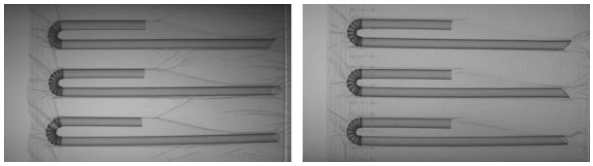

Figure 7- Samples of clear and rugged film with infrared lighting.

4.1.2 Polarized filtering imaging

This setup is based on the use of polarized filters, that only allow the light with an electrical field oscillating perpendicularly to the filter to pass through, blocking light with other polarizations, allowing the detection of physical properties that conventional imaging wouldn't be able to. In this system, a monochromatic LED was used as backlight. A CMOS monochromatic camera with a standard capability of 52 fps was used, together with a nanowire quad-polarizer filter.

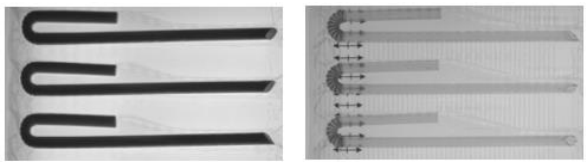

Figure 8- Samples of clear and rugged film with polarized filtering imaging.

4.2 Image preprocessing

In the images pre-processing, the area of the straws was identified and the sealed area between straws was isolated and prepared.

4.3 Feature extraction

For image classification, it is not necessary to analyze the entire image, but only a set of features that represent the required image characteristics. This compact set of features not only makes the image classification easier but also requires less computational power.

In this work, two different texture descriptors are described and their application to film sealing quality classification is studied.

4.3.1 Local binary pattern (LBP) descriptor

The local binary pattern operator is known by its efficiency, maintaining a great accuracy without requiring high computing power, reason why it is one of the most used texture descriptors.

As described by Ojala et al [12], the LBP pattern allows the representation of a gray level image texture T_{LBP} information by defining the texture in a local neighborhood as the joint distribution of the gray levels of the image pixels. This is described in equations 7 and 8, where $g_c$corresponds to the gray value of the center pixel of a local neighborhood and $g_P(p = 0, \dots, P-1)$ correspond to the gray values of *P* equally spaced pixels on a circle of radius $R_{LBP}(R_{LBP} > 0)$, forming a circularly symmetric neighbor set.

$$T_{LBP} \approx t_{LBP}\big(s(g_0 - g_c), \dots, s(g_{P-1} - g_c)\big) \quad \text{Eq. 7}$$

$$s(x) = \begin{cases} 0, & x \geq 0 \\ 1, & x < 0 \end{cases} \quad \text{Eq. 8}$$

This means that, for each pixel in the gray-level image, the central pixel is compared to the neighborhood pixels. The difference between the central pixel and each neighbor is computed and a value of "0" or "1" is obtained, resulting in a binary number being attributed to each pixel. A binary factor 2^p is

assigned to each neighbor and the original LBP value of each pixel is represented according to equation 9, making the conversion from the binary value to an integer number.

$$\mathrm{LBP} = \sum_{p=0}^{P-1} s(g_p - g_c) \times 2^p \qquad \text{Eq. 9}$$

This means that the LBP descriptor labels the pixels of an image by determining the gray levels of the P neighbors of the center pixel, according to a radius R_{LBP}. Finally, the histogram of the labels is calculated and can be utilized for texture classification.

A variation of the LBP, focused on the post-processing of the original, is defined as uniform LBP. The difference in this descriptor is that only binary patterns that are considered as uniform are taken into account in the histogram, while all the other non-uniform account only for a single position. A binary pattern is called uniform if it contains at most two bitwise transitions, with the binary string being considered circular. The resulting feature vector is obtained as a histogram of *P+1* elements of uniform patterns and one element of all other patterns summed together. This results in a significant decrease of the feature vector size, while maintaining almost all the texture related information.

Extending the LBP descriptor, it is possible to obtain a multi-resolution descriptor. As described by Ojala et al., multiresolution analysis can be accomplished by combining the information provided by multiple operators of varying radius R_{LBP} and number *P* of equally spaced pixels in that circle. Utilizing multiple LBP descriptor vectors for each image increases the amount of information obtained, which can be beneficial when it comes to its classification.

4.3.2 Gray level co-occurrence matrix

Gray level co-occurrence matrix is one of the most common used methods of texture classification. To create a GLCM, the initial gray image is first divided into a number of gray levels, where each one represents an equally sized interval of pixel intensity values, from 0 to 255. From this matrix of gray levels, a GLCM is created where the indexes of rows and columns represent the given range of the image gray levels, and the value $\mathrm{F}(i,j)$ stored at the position (i,j) is the frequency that gray levels *i* and *j* are present, at a given distance and at a given direction. After this calculation, the matrix is normalized, dividing each value by the sum of all indexes.

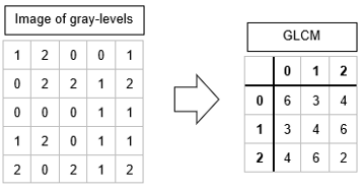

Figure 9- Example of GLCM extraction from an image divided in 3 gray-levels.

To the GLCM, it is possible to apply different statistical mathematical operations, obtaining different properties of the pixel distribution. These operators can be defined as descriptors, where each one relates to a particular visual feature of the image texture. From the application of these descriptors, an image signature is obtained, constituted by a set of numerical values, that represents one or more characteristics of it. In this work, 5 distinct descriptors are used [13].

Contrast (CON)	$\mathrm{CON} = \sum_{\mathrm{i}}\sum_{\mathrm{j}} \lvert \mathrm{i}-\mathrm{j} \rvert^2 F_{\mathrm{i,j}}$
Correlation (COR)	$COR = \sum_{\mathrm{i}}\sum_{\mathrm{j}} \frac{(i-\mu_i)(j-\mu_j)F_{\mathrm{i,j}}}{\sigma_i \sigma_j}$
Energy (ENE)	$ENE = \sum_{\mathrm{i}}\sum_{\mathrm{j}} {F_{\mathrm{i,j}}}^2$
Homogeneity (HOM)	$HOM = \sum_{\mathrm{i}}\sum_{\mathrm{j}} \frac{\mathrm{F_{i,j}}}{1+\lvert i-j \rvert}$
Entropy (ENT)	$ENT = \sum_{\mathrm{i}}\sum_{\mathrm{j}} F_{\mathrm{i,j}}(-\ln F_{\mathrm{i,j}})$

Table 1- Different descriptors used with GLCM.

When computing the GLCM from an image, multiple parameters are defined that change the matrix obtained. In this work, the variation of the number of gray level intervals, the direction and distance between pixels are analyzed.

A possible solution to increase the amount of textural information obtained from an image revolves around the extraction of multiple GLCM. This can be done by using multiple different direction and distance values, obtaining a different matrix for each pair of values. The descriptors chosen can then be applied to each individual GLCM, obtaining an image signature whose vector size equals to the number of descriptors used multiplied by the number of GLCM extracted.

4.4 Image Classification

In this work, for image classification, a multi-layer perceptron (MLP) neural network is used. This is a class of feed-forward layered networks of artificial neurons, where each neuron computes an activation function on the weighted sum of all its inputs [14].

An MLP consists of one input layer, with as many neurons as the size of the descriptor vector, one output layer, with a number of neurons equal to the number of classes, and a number of hidden intermediate layers. Each node in one layer connects with a certain weight to every node in the following layer.

For this thesis, a single hidden layer network was chosen, trained with a scaled conjugate gradient (SCG) backpropagation algorithm, known for good performances over a wide variety of problems, while maintaining a fast training time. A percentage of the images collected are used for training, another for validation and a final one for tests. The network receives a descriptor vector, corresponding to each image, as input and classifies it as acceptable or non-acceptable.

4.4.1 Method performance evaluation

In order to evaluate the quality of the method used in image classification, it is necessary to evaluate its performance.

After the image classification algorithm is applied, the images are divided into four groups, according to their predicted classification and their real classification. From this division in four groups, which represent the false positives FP, false negatives FN, true positives TP and true negatives TN, it is possible to create a confusion matrix, also known as an error matrix.

		Actual Class	
		Weak Sealing	Good Sealing
Predicted Class	Weak Sealing	**TP**	**FP**
	Good Sealing	**FN**	**TN**

Table 2- Confusion matrix model.

From this matrix it is possible to have a clear look at the algorithm performance through the calculation of the F_1 score. This indicator is equal to the harmonic mean of precision and recall, taking both false positives and false negatives into account, reaching its maximum value at 1.

$$Precision = \frac{TP}{TP + FP} \quad \text{Eq. 10}$$

$$Recall = \frac{TP}{TP + FN} \quad \text{Eq. 11}$$

$$F_1\ score = 2 \times \frac{Recall \times Precision}{Recall + Precision} \quad \text{Eq. 12}$$

5. Results

In this chapter both the results using machine vision and the pyrometers applied to sealing quality classification will be presented.

5.1 Imaging results

For image classification, the images were collected from good sealing samples, classified as good, and weak sealing and really weak sealing samples, classified as bad. These images can be divided into four groups, according to table 3.

		Nº of samples	Good to bad sealing images ratio
Clear film	Infrared imaging	710	4:1
	Polarized filtering imaging	272	1:1
Rugged film	Infrared imaging	1300	4:1
	Polarized filtering imaging	248	1:1

Table 3- Number and ratio of image samples used.

For image classification, as previously described, an MLP neural network was used. As initial parameters, it has a hidden layer size of 10 neurons and the samples, after being randomly organized, are divided into train, validation and test groups according to the ratios, respectively, of 70%, 15% and 15%. These conditions were maintained across all tests to establish a line of comparison between the different algorithms.

In order to guarantee the best results, for each test, 200 neural networks were trained, and the best performing one, with the highest F1 score, was picked. To also guarantee that the best results obtained weren't a consequence of overfitting, neural networks where the difference between the test accuracy and the train accuracy was higher than 3% were excluded.

5.1.1 LBP results

In order to estimate the best result for LBP, two parameters were varied according to the best performances obtained. These are the number of equally spaced neighborhood pixels and the radius, which is the distance in pixels between the central and the neighborhood pixels. For each group of images, the radius was varied from 1 to 20 pixels, while the number of neighborhood pixels changed from 4 to 32, in multiples of 4. The best performances for a single LBP were obtained in table 4.

		Radius	Number of pixels	F_1 score
Clear film	Infrared imaging	9	28	0.978
	Polarized filtering imaging	4	24	0.951
Rugged film	Infrared imaging	12	24	0.990
	Polarized filtering imaging	6	16	0.984

Table 4- Performance results for LBP.

However, it is still possible to combine the LBP with the best parameters with another with a different radius and number of pixels. The results can be seen in table 5. While the performances obtained from a single LBP where already high, it is still possible to verify a small increase in the F1 score obtained with the use of multiple LBP.

To evaluate if the choice for the number of neurons in the hidden layer of the neural network was correct, a test was conducted to analyze its impact in the performance obtained, whose results can be seen in figure 9. Overall, the increase of the number of artificial neurons leads to a small decrease in performance.

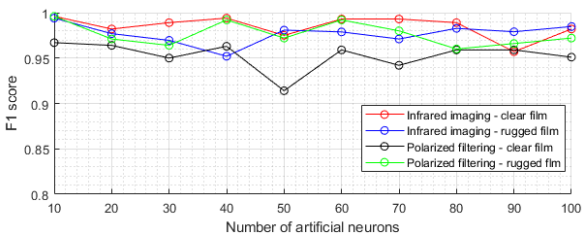

Figure 9- LBP performance variation related with the number of artificial neurons.

5.1.2 GLCM results

In order to estimate the best result for GLCM, four different parameters where varied according to the best performances. These parameters are the number of gray levels the image is divided, the direction angle and distance between pixels when computing the GLCM and the descriptors, from contrast, correlation, energy, homogeneity and entropy, used for feature extraction. The best performances obtained for a GLCM can be seen in table 6.

		Direction Angle	Distance	F_1 score
Clear film	Infrared imaging	45º	15 pixels	0.913
	Polarized filtering imaging	45º	12 pixels	0.864
Rugged film	Infrared imaging	0º	14 pixels	0.906
	Polarized filtering imaging	0º	8 pixels	0.947

Table 6- Performance results for GLCM.

Having obtained the highest performance values for a single GLCM, tests were conducted to evaluate the benefits of combining this GLCM with another with different distance and direction angle as parameters. The best results obtained can be seen in table 6. It is possible to see a significant increase in performance for all categories with the use of the more robust multiple GLCM.

Similar to before, to evaluate the impact of the number of neurons in the hidden layer of the neural network in the model performance, a test was, whose results can be seen in figure 10. It can be easily seen that the increase of the number of artificial neurons leads to a decrease in performance, which is a result of the network overfitting.

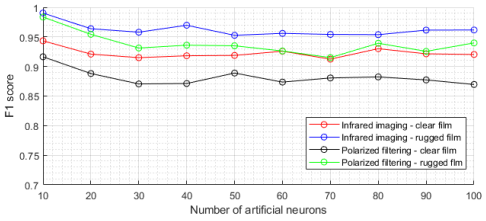

Figure 10- GLCM performance variation related with the number of artificial neurons.

5.1.3 Imaging results comparison

Despite the great performances achieved with the GLCM, the local binary pattern takes the win for all four groups of images.

Comparing both image acquisition systems, when it comes to the clear film, the infrared imaging is clearly the best option. For the rugged film, however, the polarized filtering imaging presents a small edge. It is important to mention, however, that for the rugged film the number of images from polarized filtering used was much lower.

Having achieved an F1 score of 0.996 for both types of films means, in practical terms, that the algorithm predicts the image classification with an accuracy of 99.5%, or that 1 in 200 images will be predicted wrong. While this seems like an optimal result, in a practical application in an industrial setting at high production speeds, 1 in 200 wrong predictions has a major impact.

For an application in industrial environment, there is another parameter that needs to be taken into account, which is the algorithm's computational time. In table 8 it is possible to see the computational times for the different algorithms, which include all the steps from image preparation, features extraction and classification.

		Computational time [s]	
		mean	***σ***
LBP	Single	0.616	0.094
	Multiple	0.939	0.152
GLCM	Single	0.289	0.024
	Multiple	0.343	0.018

Table 8- Computational times.

Overall, it is possible to see that the GLCM descriptor is significantly faster than the LBP, with a computational time 53% lower if we compare the single algorithms, or an even higher 63% time reduction for the multiple descriptors. Despite having a worse performance, in cases where low computational speed is essential, the GLCM presents a great advantage.

		LBP 1		LBP 2		F_1 score
		Radius	Number of pixels	Radius	Number of pixels	
Clear film	Infrared imaging	9 pixels	28 pixels	13 pixels	4 pixels	0.996
	Polarized filtering imaging	4 pixels	24 pixels	5 pixels	24 pixels	0.967
Rugged film	Infrared imaging	12 pixels	24 pixels	19 pixels	28 pixels	0.994
	Polarized filtering imaging	6 pixels	16 pixels	8 pixels	4 pixels	0.996

Table 5- Performance results for multiple LBP.

		GLCM 1		GLCM 2		F_1 score
		Direction angle	Distance	Direction angle	Distance	
Clear film	Infrared imaging	45º	15 pixels	0º	6 pixels	0.943
	Polarized filtering imaging	45º	12 pixels	0º	17 pixels	0.916
Rugged film	Infrared imaging	0º	14 pixels	90º	17 pixels	0.990
	Polarized filtering imaging	0º	8 pixels	45º	4 pixels	0.984

Table 7- Performance results for multiple GLCM.

5.2 Pyrometer experimental results

To analyze the real response of the pyrometer in the industrial environment, the sensor was installed in two different machines, for each type of film, in the straw factory, placed right after the sealing process, normal to the film, at 10mm.

5.2.1 Normal production conditions

Assuming the peak and valley film average temperatures, it is possible to estimate the pyrometer model, and compare it to the experimental data obtained.

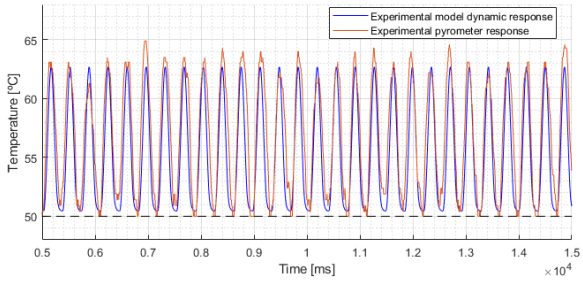

Figure 11- Comparison between theoretical model and experimental data.

Despite the theoretical model proposed being a simplified representation of the film temperature variation, it is possible to observe that the experimental data obtained shows a very similar behavior to the model, obtaining a mean error of 1.89ºC, with a standard deviation of 2.95 ºC.

5.2.2 Moving average filter

In order to correlate the pyrometer temperature measured with the seal quality of the film, the only temperature values necessary to analyze are the ones related to the film sealed surface, which correspond to the peak temperature values in each iteration. However, these peak temperature values can fluctuate. To contradict this, a moving average filter can be applied to the data values related to temperature peaks. This filter operates by averaging a number of points, from the input signal, to estimate each point in the output signal. A number of 9 previous peaks was chosen for averaging.

5.2.3 Experimental results

In order to observe if the pyrometer was capable of detecting when problems with the sealing quality occur, two sets of tests were conducted.

In the first type, with the machine always working, the parameters values were slowly dropped allowing the observation of the pyrometer response in real time, for both temperature and pressure variation independently, as seen in figures 12 e 13 for rugged film.

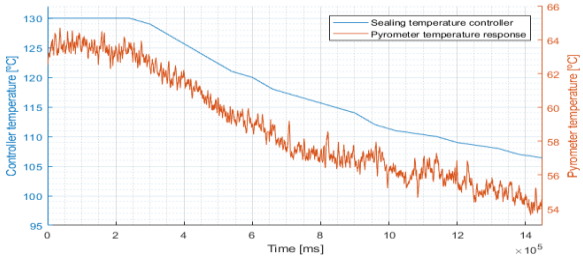

Figure 12- Pyrometer response to temperature variation for rugged film.

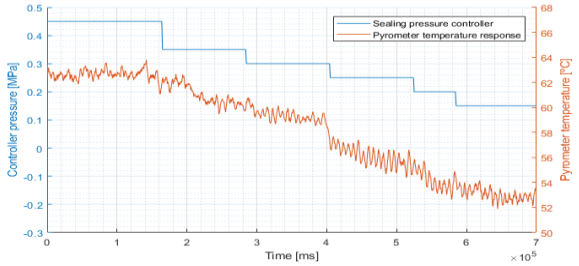

Figure 13- Pyrometer response to pressure variation for rugged film.

It is clearly possible to see the pyrometer proportional response to the parameters change.

The second type of tests were conducted with fixed parameter values, to study the pyrometer response in these conditions. The values chosen correspond to good and weak sealing previously defined.

For both types of film and changes in the temperature and pressure parameters it was possible to make a clear distinction between acceptable and not acceptable sealing temperature measurements in both films, as seen in tables 9 and 10.

Type of film	Controller pressure [MPa]	Quality of sealing	Pyrometer temperature value	
			mean	max deviation
Clear film (at 115 ºC)	0.50	Good sealing	67.21	1.68
	0.30	Weak sealing	63.50	1.74
Rugged film (at 130 ºC)	0.50	Good sealing	63.44	1.96
	0.30	Weak sealing	59.03	2.07

Table 9- Pyrometer response for different pressure values.

Type of film	Controller temperature [ºC]	Quality of sealing	Pyrometer temperature value	
			mean	max deviation
Clear film (at 0.5 MPa)	115	Good sealing	67.21	1.46
	105	Weak sealing	63.82	1.71
Rugged film (at 0.5 MPa)	130	Good sealing	63.44	1.94
	120	Weak sealing	58.74	1.79

Table 10- Pyrometer response for temperature values.

With these tests it is proven the capability of using the measurement of the sealed film surface temperature, for both types of films, with a pyrometer sensor, as a way of evaluating the film sealing strength.

6. Conclusions

6.1 Achievements

This work proposes two distinct systems for inspection of BOPP film sealing quality in straw packaging. The main goal is to have an in-line system capable of inspecting all the products produced and detecting possible sealing defects produced, for two different types of film, while being viable to be implemented in an industrial environment.

First, an analysis of the heat-sealing process and parameters was presented. Sealed film samples for different production parameter values were produced and subjected to a peel test for measurement of their seal strength. The critical area of the film was identified, and the samples were classified according to their sealing quality.

A hypothesis was presented relating the seal quality with the temperature of the film after sealing. A pyrometer device specific for thin plastic film was analyzed. Theoretical and experimental models for the pyrometer were presented, together with the estimation of the model for film temperature variation. The pyrometer was then tested in a real application, validating the theoretical film temperature variation model presented. A moving average filter was introduced for data processing. The experimental results obtained with the pyrometer in abnormal production showed that the film temperature measured is directly related with the change in the production parameters that govern the sealing process, proving the hypothesis that it can be related with sealing quality. It is also clearly possible to make a distinction between the different sealing quality classifications according to the temperature measured, for both types of film, proving the capability of this system in inspecting BOPP film sealing quality.

A solution for sealing quality inspection based on machine vision was also presented. Two different imaging systems, one based on infrared lighting and the other on polarized filtering, were used to collect images from the samples obtained for different production conditions. Two textural descriptors were proposed for image features extraction, based on the local binary pattern and the gray level co-occurrence matrix and for classification, a multi-layer perceptron neural network was used.

Good results were obtained, with F1 scores very close to one for both types of film. showing the good capability of the textural descriptors in extracting from the images the necessary information related to its sealing properties. Comparing the two descriptors performances, the local binary pattern achieves a higher performance for all the systems. Comparing, however, the computational times, the GLCM descriptor is much faster than the LBP.

Overall, with this work it was possible to achieve the main objective of identifying a system for in-line inspection of BOPP film sealing quality in straw packaging.

6.2 Future work

A route to explore would be the application of a thermographic camera specific for thin PP film, since an area analysis of the sealed film surface in real time would bring major advantages when compared to the point temperature measurement of pyrometers, allowing us to pinpoint the defect area and more easily identify the root cause of the problem.

Another area to explore would be to test different image acquisition systems, with new and improved cameras being constantly developed. Different classification algorithms could also prove to be more effective, especially with the constant new developments in artificial intelligence capabilities for image recognition and classification.

References

[1] B. Morris, *The science and technology of flexible packaging: multilayer films from resin and process to end use*. Boston, MA: Elsevier, 2016.

[2] S. Ebnesajjad, *Plastic films in food packaging materials, technology and applications*. Amsterdam: Elsevier, William Andrew, 2013.

[3] S. E. M. Selke and J. D. Culter, *Plastics packaging: properties, processing, applications, and regulations*, 3rd edition. Munich : Hanser Publishers ; Cincinnati: Hanser Publications, 2016.

[4] M. A. Pascall, J. Richtsmeier, J. Riemer, and B. Farahbakhsh, “Non-destructive packaging seal strength analysis and leak detection using ultrasonic imaging,” *Packaging Technology and Science*, vol. 15, no. 6, pp. 275–285, Nov. 2002.

[5] B. Ostyn, P. Darius, J. De Baerdemaeker, and B. De Ketelaere, “Statistical Monitoring of a Sealing Process by Means of Multivariate Accelerometer Data,” *Quality Engineering*, vol. 19, no. 4, pp. 299–310, Oct. 2007.

[6] Y. S. Song, M. Gera, B. Jain, and J. L. Koontz, “Evaluation of a Non-destructive High-voltage Technique for the Detection of Pinhole Leaks in Flexible and Semi-rigid Packages for Foods: High-voltage leak detection for food packages,” *Packaging Technology and Science*, vol. 27, no. 6, pp. 423–436, Jun. 2014.

[7] Z. Shuangyang, “Fast Inspection of Food Packing Seals Using Machine Vision,” in *2010 International Conference on Digital Manufacturing & Automation*, Changcha, TBD, China, 2010, pp. 724–726.

[8] M. Barnes, M. Dudbridge, and T. Duckett, “Polarised light stress analysis and laser scatter imaging for non-contact inspection of heat seals in food trays,” *Journal of Food Engineering*, vol. 112, no. 3, pp. 183–190, Oct. 2012.

[9] K. D’huys, W. Saeys, and B. De Ketelaere, “Active Infrared Thermography for Seal Contamination Detection in Heat-Sealed Food Packaging,” *Journal of Imaging*, vol. 2, no. 4, p. 33, Nov. 2016.

[10] T. L. Bergman, A. Lavine, and F. P. Incropera, *Fundamentals of heat and mass transfer.* 2017.

[11] D. P. DeWitt and G. D. Nutter, Eds., *Theory and practice of radiation thermometry*. New York: Wiley, 1988.

[12] T. Ojala and M. Pietikainen, “A comparative study of texture measures with classification based on feature distributions,” *Pattern recognition 29.1*, pp. 51–59, 1996.

[13] R. M. Haralick, K. Shanmugam, and I. Dinstein, “Textural Features for Image Classification,” *IEEE Transactions on Systems, Man, and Cybernetics*, vol. SMC-3, no. 6, pp. 610–621, Nov. 1973.

[14] M. Sonka, V. Hlavac, and R. Boyle, *Image processing, analysis, and machine vision*, 3. ed. Stamford, Conn.: Cengage Learning, 2008.